Supporting information for

Is deprotonation of the oxygen-evolving complex of photosystem II during the $S_1 \rightarrow S_2$ transition suppressed by proton quantum delocalization?

Ke R. Yang,[a] K. V. Lakshmi,[b] Gary W. Brudvig,[a] and Victor S. Batista[a,*]

[a] Department of Chemistry, Yale University, New Haven, CT 06520-8107, USA

[b] Department of Chemistry and Chemical Biology and The Baruch '60 Center for Biochemical Solar Energy, Rensselaer Polytechnic Institute, Troy, NY 12180, USA

Email: *victor.batista@yale.edu*

Table of Contents

1. Computational details

1.1 Model selection of the OEC:

The computational model of the OEC of PSII was constructed from our previous QM/MM model of the S_2 state[1] based on the 1.9 Å resolution crystal structure (PDB: 3ARC).[2] We included amino-acid residues as well as water molecules within 15 Å of the $CaMn_4O_5$ cluster and two chloride ions near the OEC. Neutral capping groups (ACE/NME) were used to cap the peptide chains at the boundary. All of the acidic residues (Asp and Glu) were modeled as anions. D1-His337, D1-Arg357, and D2-Lys317 were modeled as protonated. Sodium counter ions were added to neutralize the system.

The final protein selection includes the following residues (capping residues in parenthesis use only the backbone atoms):

D1 (*chain A*): (57)-58-67-(68), (81)-82-91-(92), (107)-108-112-(113), (155)-156-192-(193), (289)-290-298-(299), (323)-324-344:C-terminus

CP43 (*chain C*): (290)-291-(292), (305)-306-314-(315), (334)-335-337-(338), (341)-342-(343), (350)-351-358-(359), (398)-399-402-(403), (408)-409-413-(414)

D2 (*chain D*): (311)-312-321-(322), (347)-348-352:C-terminus D1

1.2 QM/MM structural optimization:

The QM/MM optimization for the S_2 state structures was performed using a two-layer ONIOM method[3-4] with H link-atoms as implemented in the Gaussian 16 software package (Rev. B.01).[5] The QM region includes the OEC, all directly ligated side chains (D1-D170, D1-E189, D1-H332, D1-E333, D1-D342, and CP43-E354), the C-terminus of D1-A344, hydrogen-bonded residues D1-D61, D1-S169, D1-G171, D1-N181, D1-H337 and CP-R357, D2-K317, 13 water

molecules, and a Cl^- cofactor (**Figure S1**). A much larger QM region was used in comparison to our previous study in order to include a complete hydrogen-bonding network around the OEC which is terminated by amino-acid residues and Cl^- cofactor (See **Section S2**). The QM region was treated using the B3LYP functional[6] with a mixed double zeta (MDZ) basis set, the Lanl2DZ pseudopotential and basis set for Ca and Mn,[7] the 6-31G(d) basis for O and Cl,[8-9] and the 6-31G basis set for H, C, and N.[8-9] The AMBER 98 force field[10] was used to model the MM region. The electronic embedding ONIOM approach was used during the geometry optimization to provide a better description of the electrostatic interaction between the QM and MM region by allowing the QM region to be polarized by the MM partial charges. All of the atoms were allowed to relax during QM/MM optimization with the exception of the chloride ions, neutral capping groups (ACE/NME), and oxygen atoms of water molecules in the MM region.

1.3 EXAFS simulation

The classical EXAFS equation is shown below

$$\chi(k) = \sum_{j}^{\text{paths}} N_j S_0^2 \frac{|f(k)|}{kR_j^2} \sin(2kR_j + 2\delta_c + \phi) e^{-2R_j/\lambda(k)} e^{-2\sigma^2 k^2}, \quad \text{(S1)}$$

where j goes over all scattering paths, k is the momentum vector, $2\delta_c + \phi$ is the phase shift. The structural parameters are the interatomic distances R_j, the coordination number (or number of equivalent scatterers) N_j, and the temperature-dependent root-mean-square (rms) fluctuation in bond length σ, which also includes effects due to structural disorder. Additionally, $f(k) = \left| f^{\text{eff}}(k) \right| e^{i\phi(k)}$ is the backscattering amplitude, δ_c is central-atom partial-wave phase shift of the final state, and $\lambda(k)$ is the energy-dependent XAFS mean free path. S_0^2 is the overall amplitude factor.

Isotropic Mn K-edge EXAFS spectra of the structures considered were calculated using the *ab initio* real space Green function approach as implemented in the FEFF6 program[11] and the IFEFFIT code.[12] The experimental EXAFS data $\chi(E)$, that is the fractional change in absorption coefficient of Mn atoms induced by neighboring atoms, are converted into momentum (k) space using the transformation $k = \left[\frac{2m_e}{(h/2\pi)^2}(E - E_0) \right]^{1/2}$, where m_e is the mass of the electron, h is the Planck's constant, and E_0 is the energy of the absorption edge (E_0) of Mn element (6539.0 eV) which may shift slightly according to its oxidation state and chemical environment.

The coordinates of atoms in the QM region of the QM/MM optimized structures of various S_2 models were used to calculate the scattering amplitude, phase shift, EXAFS mean free path in Eq. (S1). All of the calculations using Feff6 were performed using the following parameters: "NLEG 8", and "CRITERIA 4.0 2.5" and "RMAX 5.5". The Debye-Waller factors (DWF) σ^2 were set to be 0.001Å^2 for first coordination paths (Mn–O or Mn–N path) and 0.002 Å^2 for other scattering paths. A fractional cosine-square (Hanning) window with $\Delta k = 1$ was applied to the experimental and calculated EXAFS data. A grid of k points equally spaced at 0.05 Å^{-1} was used for the Fourier transformation (FT) of in the k range of 4.0-10.5 Å^{-1}. The overall amplitude factor S_0^2 is adjusted to match the calculated FT magnitude and EXAFS χk^3 values with the experimental data, while the edge shift ΔE_0 is varied to minimize the deviation between the calculated and experimental $\chi(k)$. The simulated EXAFS spectra of models A, B, and C, along with the experimental EXAFS spectra, are shown in Figure S2.

1.4 Solving the proton Schrodinger equation:

We approximate the proton shared between W_1 and D1-D61 as a particle in a 1D potential well. The potential energy curve of the proton is obtained by translocating the proton between the O atom of W_1 and O atom in D1-D61. The bond lengths of O–H are frozen during the partial optimization.

The Schrodinger equation of the proton is:

$$H\psi(x) = \left(-\frac{\hbar^2}{2m}\frac{d^2}{dx^2} + V(x) \right)\psi(x) = E\psi(x), \quad \text{(S-2)}$$

where x is the distance between the proton and the O atom in D1-D61 and $V(x)$ is obtained from by the cubic spline interpolation of the energies from our scan calculations, the mass of the particle is chosen to be the mass of proton (1836 in atomic units). The Schrodinger equation was solved using the Fourier grid Hamiltonian method.[13]

To investigate the effects of basis sets and dispersion interactions on the calculated double-well potentials and the vibrational states of the shared proton, we performed single point calculation along the O–H coordinate using the B3LYP functional[6] with a larger basis set to investigate the effect of diffuse and polarization basis functions (**Figures S3** and **S4**). More specifically, the QM regions were treated using the B3LYP functional with the Lanl2DZ pseudopotential and basis set for Ca and Mn,[7] the 6-31+G(d) basis for O and Cl,[8-9, 14-15] and the 6-31G(d) basis set for H, C, and N.[8-9] The effect of dispersion interactions was considered by using Grimme's third version of empirical dispersion correction (GD3)[16] and the results are shown in **Figures S5** and **S6**. The shared proton is always described by a double-well potential along the O–H coordinate regardless the methods we used to calculate the potential energy curve and the vibrational state wave functions are delocalized along the O–H coordinate.

We also considered the harmonic vibrational frequencies of the proton at the bottoms of each single-well (**Figure S7**). The harmonic frequencies of the proton at the carboxyl group in D1-D61 and W1 are 2816 and 2641 cm^{-1}, corresponding to ZPEs of 4.0 and 3.8 kcal/mol, respectively. The harmonic frequencies of O–H stretching are already much smaller than the typical O–H stretching frequency in H_2O or a carboxyl group of ~ 3000 cm^{-1} due to the strong hydrogen-bond interaction between W1 and the carboxyl group in D1-D61. The vibrational frequencies are further reduced by considering the quantum delocalization along the O–H coordinate (**Figure 3**).

2. Hydrogen-bonding network around OEC

We considered different hydrogen-bonding patterns of water molecules that are present around the OEC in the X-ray crystal structure. Water molecules can serve as both hydrogen-bond donors and acceptors. Therefore, there is some ambiguity on the hydrogen-bonding pattern around the OEC. The protein backbone, amino-acid side chains and cofactors, on the contrary, play relatively simple roles in hydrogen-bond formation. For example, the carbonyl O atoms in the backbone only serve as hydrogen-bond acceptors while the amide groups in the backbone serve as hydrogen-bond acceptors. We extended the QM region from our previous QM/MM model of the S_2 state. More specifically, we include the water molecules in the X-ray crystal structure that are near the OEC and extend the hydrogen-bonding network until the hydrogen bonds were terminated by amino-acid residues or cofactors. It is important to note that the terminal amino-acid residues such as N181, F182, Y161, K317, D61, S169, D170, E189, R357 and the Cl^- cofactor are all highly conserved. Therefore, it is reasonable to assume that they act as a scaffold to maintain a well-defined hydrogen-bonding network for efficient functioning of the OEC.

Two additional water molecules in the X-ray crystal structure that have not been considered quantum mechanically in most previous theoretical modeling are also included in our QM region to form a complete hydrogen-bonding network. These are named W_{10} and W_{11}, where W_{10} forms a hydrogen bond with the backbone carbonyl group of S169 and G171 and W_{11} forms a hydrogen bond with W_{10} and N181.

While studying the hydrogen-bonding network around the OEC, we noticed that there is a tetrameric water motif between W_2 and W_3 that is comprised of W_3, W_5, W_6, and W_7. The tetrameric water motif connects W_2 and D1-Y161 which may play an important role in the photo-induced proton release upon oxidation of D1-Y161 during the S-state transitions through hydrogen-bond rearrangement.

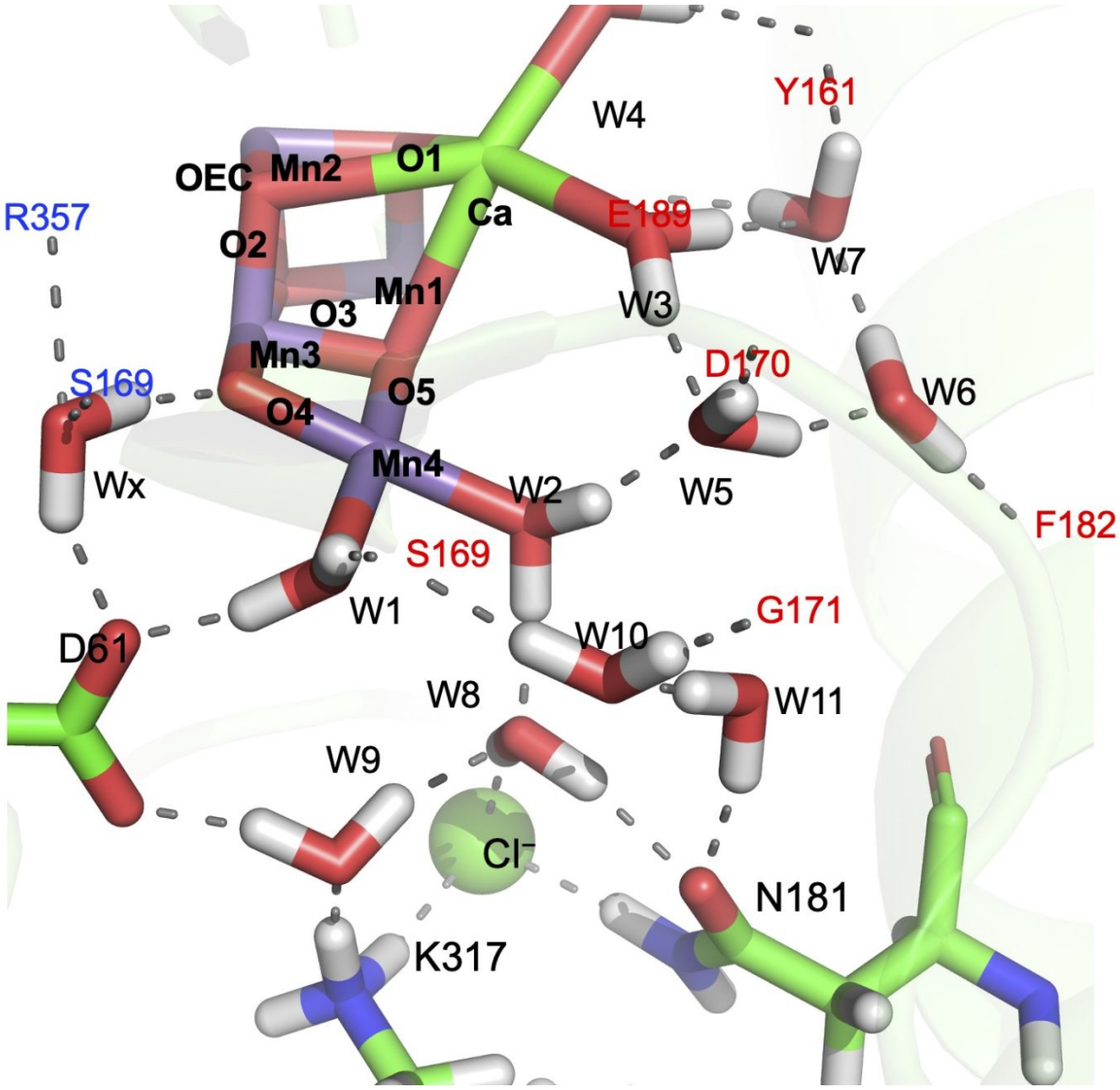

Figure S1. The hydrogen-bonding network formed by water molecules and key amino-acid residues and Cl^- cofactor around the OEC.

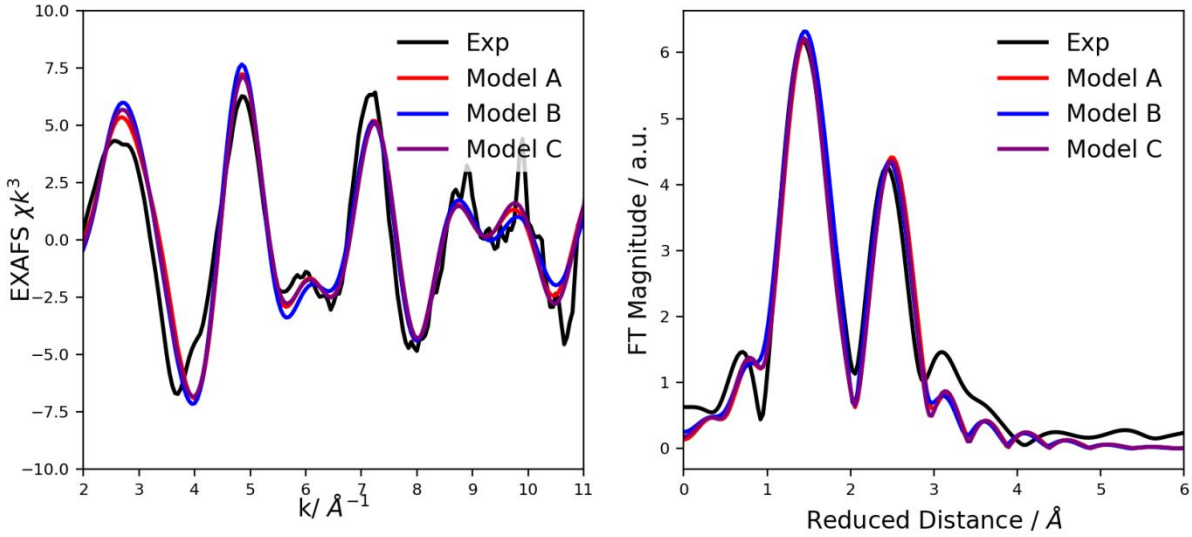

Figure S2. Simulated EXAFS spectrum of each of the S_2 state structures with different protonation states that are shown in **Figure 2A-C**.

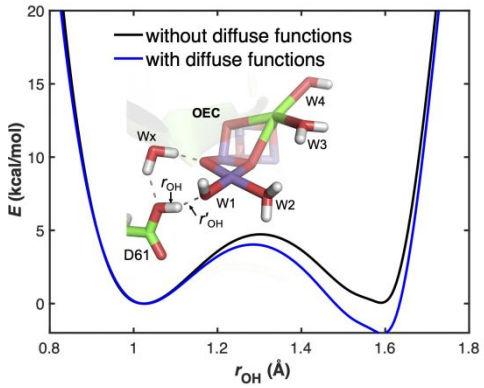

Figure S3. Potential energy curves calculated without and with diffuse and polarization functions along the O–H coordinate.

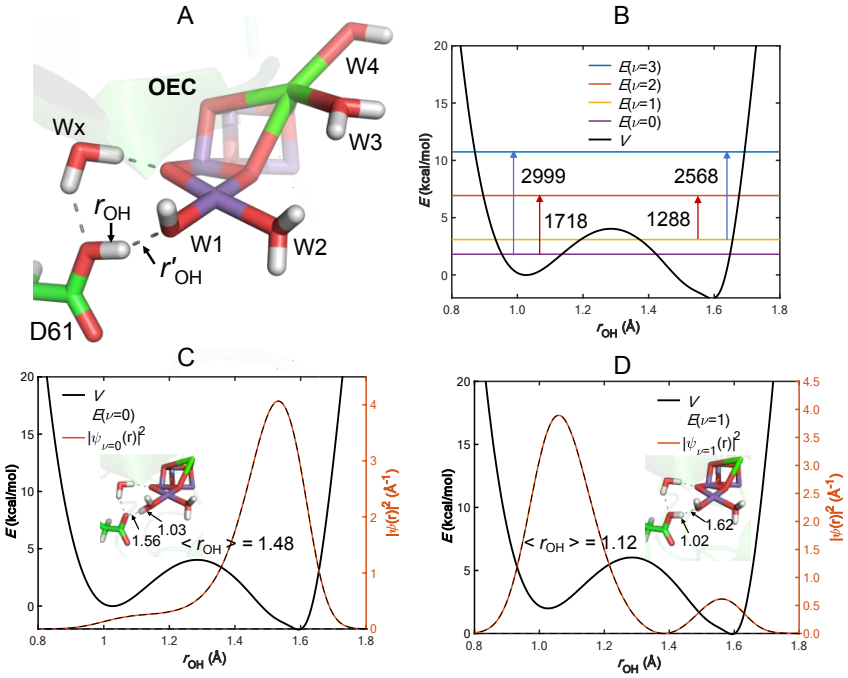

Figure S4. A quantum-delocalized proton between W_1 and D1-D61 in the S_2 state of the OEC on potential energy curve calculated using a larger basis set included both polarization and diffuse basis functions. **A**. The structure of D1-D61 and water molecules in the OEC with r_{OH} and r'_{OH} denoting distances between the quantum proton and O atoms in D1-D61 and W_1, respectively; **B**. The potential energy curve along r_{OH}. The energy eigenvalues of the four lowest vibrational states and excitation energies between different vibrational states are in cm^{-1}; Probability density $|\psi(r)|^2$ of the ground (**C**) and first excited (**D**) vibrational states. The expectation values of r_{OH} are in Å. The inset structures in **C** and **D** correspond to the classical structures under the Born-Oppenheimer approximation with the proton located at D1-D61 and W_1, respectively. The expectation values of r_{OH}, evaluated from quantum mechanical vibrational wave functions deviate significantly from the r_{OH} in the classical structures, indicating the strong quantum delocalized nature of the proton that is shared between W_1 and D1-D61.

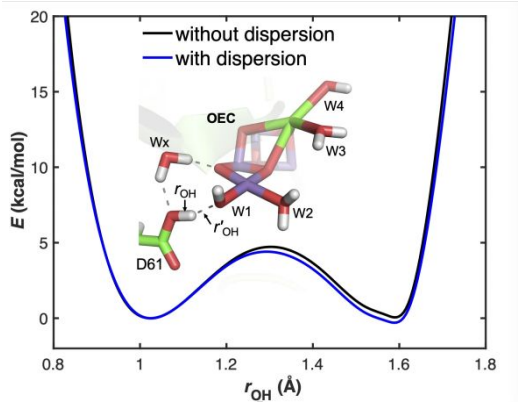

Figure S5. Potential energy curves calculated without and with Grimme's empirical dispersion (GD3) along the O–H coordinate.

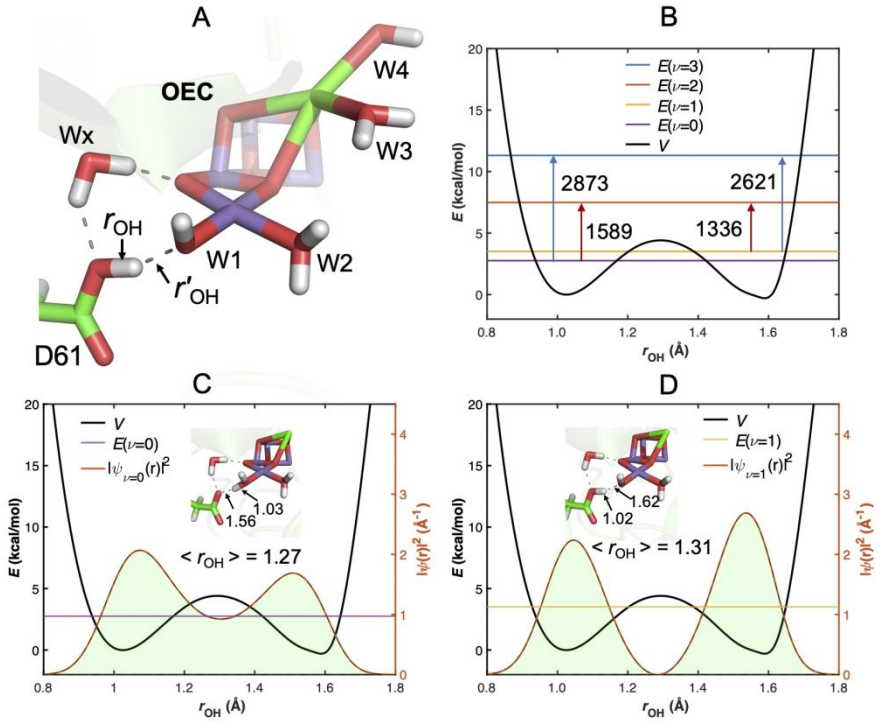

Figure S6. A quantum-delocalized proton between W_1 and D1-D61 in the S_2 state of the OEC on the potential energy curve calculated using B3LYP with Grimme's empirical dispersion correction (GD3). **A**. The structure of D1-D61 and water molecules in the OEC with r_{OH} and r'_{OH} denoting distances between the quantum proton and O atoms in D1-D61 and W_1, respectively; **B**. The potential energy curve along r_{OH}. The energy eigenvalues of the four lowest vibrational states and excitation energies between different vibrational states are in cm^{-1}; Probability density $|\psi(r)|^2$ of the ground (**C**) and first excited (**D**) vibrational states. The expectation values of r_{OH} are in Å. The inset structures in **C** and **D** correspond to the classical structures under the Born-Oppenheimer approximation with the proton located at D1-D61 and W_1, respectively. The expectation values of r_{OH}, evaluated from quantum mechanical vibrational wave functions deviate significantly from the r_{OH} in the classical structures, indicating the strong quantum delocalized nature of the proton that is shared between W_1 and D1-D61.

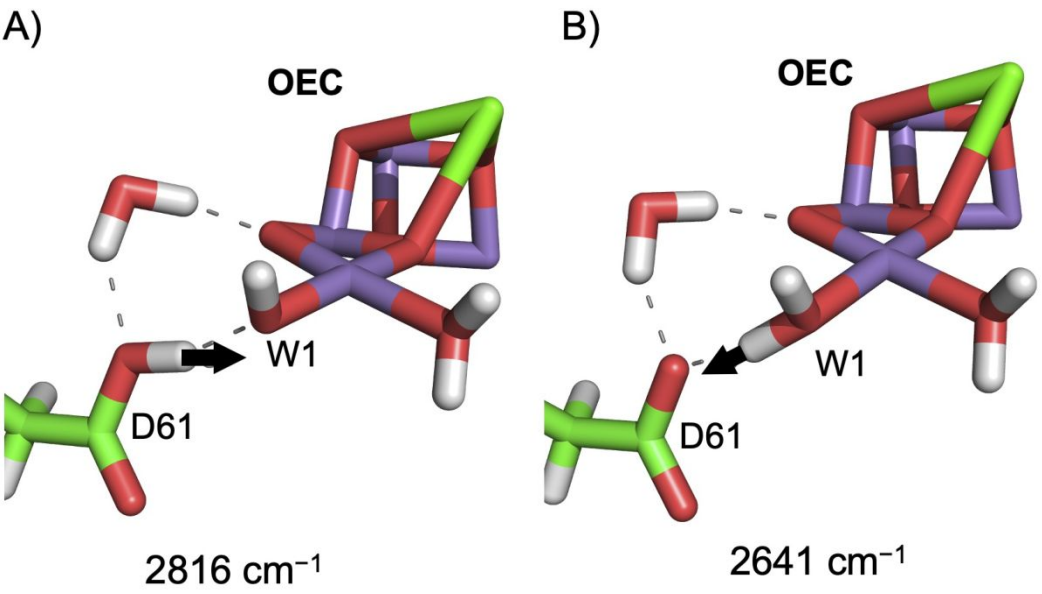

Figure S7. Harmonic vibrational frequencies of O–H stretching for classical proton states with the proton located at **A**) the carboxyl group of D1-D61 and **B**) W1. The black arrows indicate the directions of the proton motion in O–H stretching modes.

3. Magnetic structure and determination of proton hyperfine coupling constants from broken symmetry solutions

We studied the magnetic structures and proton hyperfine coupling constants of the dimanganese(III,IV) di-μ-oxo di-terpyridine di-aqua (Mn-terpy) model complex and various models of the S_2 state using the broken-symmetry approach with the software program, ORCA (Version 4.0.1).[17] Initial broken symmetry guesses were constructed using the "flipspin" feature of the ORCA program from converged high-spin solutions.

The geometries of the Mn-terpy model complex (with and without explicit water molecules) were optimized using the B3LYP functional[6] with the scalar relativistic effects considered by the zeroth-order regular approximation (ZORA) Hamiltonian.[18-19] ZORA-adapted segmented all-electron relativistically contracted (SARC) basis sets ZORA-def2-SVP were employed for all atoms. The resolution of identity (RI) approximation, along with de-contracted auxiliary def2-SVP/J coulomb-fitting basis sets, was invoked to reduce the computational time.[20-22] Dispersion interactions were considered by Grimme's third-generation (D3) semiempirical van der Waals corrections.[16, 23] Increased integration grids (Grid4 and GridX5 in ORCA convention) and tight SCF convergence criteria were used throughout the calculations. The COSMO solvation model with a dielectric constant of 80.5 is used to account for the aqueous environment of the Mn-terpy dimer. The B3LYP-D3 optimized geometries of Mn-terpy were used to study the magnetic structure and served as a benchmark for the calculated proton hyperfine coupling constants of water-derived ligands at the Mn(III) and Mn(IV) centers.

The QM/MM optimized structures of the various models of the OEC in the S_2 state were used to study their magnetic structures and proton hyperfine coupling constants. Only the atoms in the QM region were used in the magnetic structures and hyperfine coupling constants. The

dangling C and N atoms were capped with H atoms with $d_{C–H}$ (1.09 Å) and $d_{N–H}$ (1.02 Å). The COSMO solvation model with a dielectric constant of 8.0 was used to account for the protein environment around the OEC.[24-25]

Calculations of magnetic structures and proton hyperfine coupling constants were performed using the B3LYP functional and the basis sets developed by Neese *et al.* based on the SARC def2-TZVP for the Mn, N, and O atoms and def2-TZVP(-f) for all other atoms.[26] The integration grids were increased to finer grids (Finalgrid6 and GridX5 in ORCA convention). Exchange coupling constants were calculated from the energies of high-spin and broken-symmetry (BS) solutions. The exchange coupling constants were used to calculate spin projector factor to extract isotropic hyperfine coupling constants from "raw" calculated BS-DFT hyperfine coupling constants.[27]

For a magnetic system with several local magnetic centers, the magnetic structure can be described by the Heisenberg-Dirac-van Vleck (HDvV) Hamiltonian:

$$H_{\mathrm{HDvV}} = -2\sum_{i<j} J_{ij}\overrightarrow{S_i}\cdot\overrightarrow{S_j}\,. \qquad \text{(S2)}$$

Following the methodology proposed by Pantazis *et al.*,[27] the isotropic hyperfine coupling constants can be extracted from the "raw" calculated BS-DFT hyperfine coupling constants:

$$A_{\mathrm{iso}}^{(i)} = \pm A_{\mathrm{iso,BS}}^{(i)}\left(\frac{\langle S_Z\rangle_{\mathrm{BS}}}{S_{\mathrm{A}}}\right) c_{\mathrm{A}}, \qquad \text{(S3)}$$

where $\langle S_Z\rangle_{\mathrm{BS}}$ refers to the total M_S of the BS-DFT solution with s_{A} denoting the formal spin at site A, c_{A} is the spin projection coefficient at site A, and nucleus *i* belongs to site A. c_{A} is calculated using the equation:

$$c_{\mathrm{A}} = \frac{\langle S_{Z,\mathrm{A}}\rangle_{\mathrm{GS}}}{S_{\mathrm{tot}}}, \qquad \text{(S4)}$$

where $\langle S_{Z,\mathrm{A}}\rangle_{\mathrm{GS}}$ refers to the expectation value of $\widehat{S_Z}$ for site A in the ground state obtaining by diagonalizing the Heisenberg-Dirac-van Vleck (HDvV) Hamiltonian.

$$\langle S_{Z,\mathrm{A}}\rangle_{\mathrm{GS}} = \sum_k \left|c_0^k\right|^2 M_{S,\mathrm{A}}^k, \qquad \text{(S5)}$$

3.1 Mn-terpy model complex

For the Mn-terpy model complex with a mixed-valent Mn(III) and Mn(IV) core (**Figure S8**), there is one high-spin (HS) solution (4α3α (M_S = 7/2)) and one broken (BS-DFT) solution (4α3β (M_S =1/2)). The energy of the HS and BS-DFT solution can be used to extract the exchange coupling constant between the two Mn centers and deduce the spin project factors ($\left(\frac{\langle S_Z\rangle_{\mathrm{BS}}}{S_{\mathrm{A}}}\right) c_{\mathrm{A}}$ = 1/2 for the Mn(III) center and 1/3 for the Mn(IV) center).

The calculated isotropic proton hyperfine coupling constants of Mn-terpy without and with two explicit water molecules are shown in **Table S1**. The protons in the water ligand coordinated to Mn(III) have larger isotropic hyperfine coupling constants than those in the water ligated to Mn(IV). However, in the absence of the two explicit water molecules hydrogen-bonding to the more acidic Mn(IV)–OH_2, the agreement of calculated proton HFCs of water coordinated to Mn(IV) is not good, suggesting proton HFCs are sensitive to hydrogen-bonding interactions.

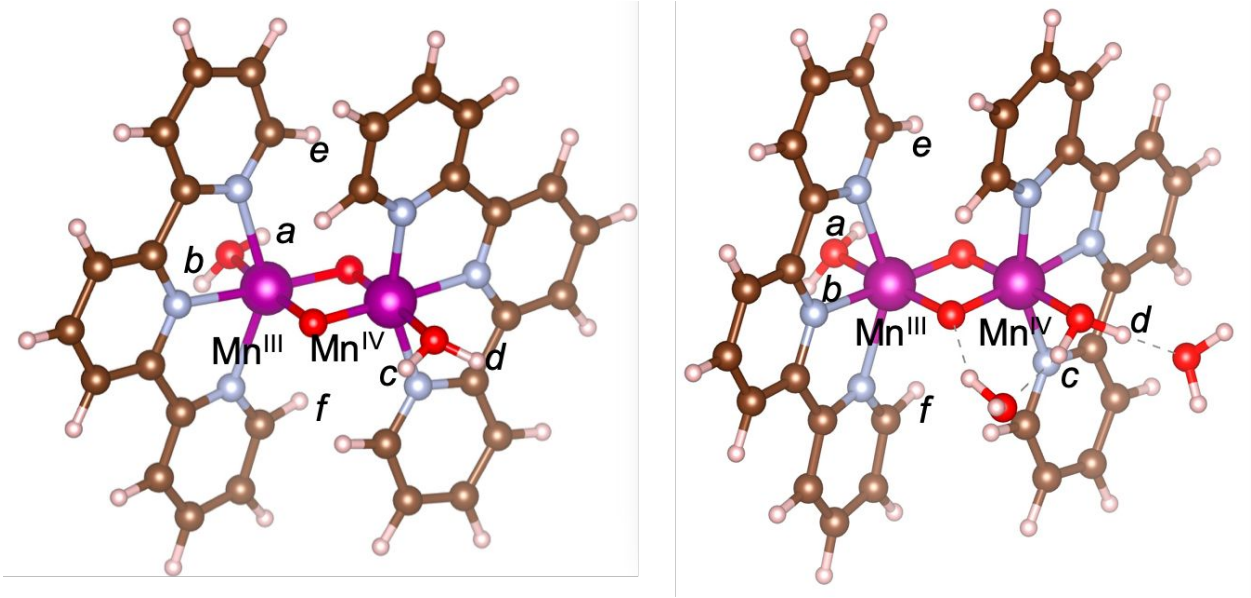

Figure S8. Optimized structures of Mn-terpy model complex without and with two explicit hydrogen-bond acceptors to the acidic Mn(IV)-OH_2.

Table S1. Calculated and experimental isotropic proton hyperfine coupling constants (in MHz) of the Mn-terpy model complex.

Hydrogen Atoms	**0 H_2O**	**2 H_2O**	**Expt.**
Ha	2.5	2.5	2.5 ± 0.4
Hb	3.0	3.2	2.5 ± 0.4
Hc	-1.6	-2.3	-2.1 ± 0.2
Hd	-0.5	1.1	-1.9 ± 0.2
He	1.5	1.5	1.1 ± 0.3
Hf	1.6	1.6	1.1 ± 0.3

3.1 OEC in the S_2 state

There are four Mn centers in OEC, namely Mn1, Mn2, Mn3, and Mn4. The couplings between the four Mn centers are shown in **Figure S9**. In the S_2 state, Mn1, Mn2, Mn3, and Mn4 are in oxidation state III, IV, IV, and IV, respectively. Therefore, the possible high-spin and broken symmetry solutions (2^{n-1}) are:

4α3α3α3α	(M_S=13/2)
4α3α3α3β	(M_S=7/2)
4α3α3β3α	(M_S=7/2)
4α3β3α3α	(M_S=7/2)
4β3α3α3α	(M_S=5/2)
4α3α3β3β	(M_S=1/2)
4α3β3α3β	(M_S=1/2)
4α3β3β3α	(M_S=1/2)

The respective energy of the 1 HS and 7 BS solution can be calculated with ORCA. The 6 exchange coupling constants and the 7 relative energies of the eight states can be related by the HDvV Hamiltonian (Eq. S2). The exchange coupling constants were extracted using single-value decomposition (SVD) implemented in Matlab for the three protonation state models, **A**, **B**, and **C**, (**Table S2**). The exchange coupling constants can be used to diagonalize the Heisenberg-Dirac-van Vleck (HDvV) Hamiltonian and obtain the spin-projectors of the different models (**Tables S3-S5**) to enable the extraction of the proton HFCs from raw broken symmetry calculated proton HFCs (**Table S6**).

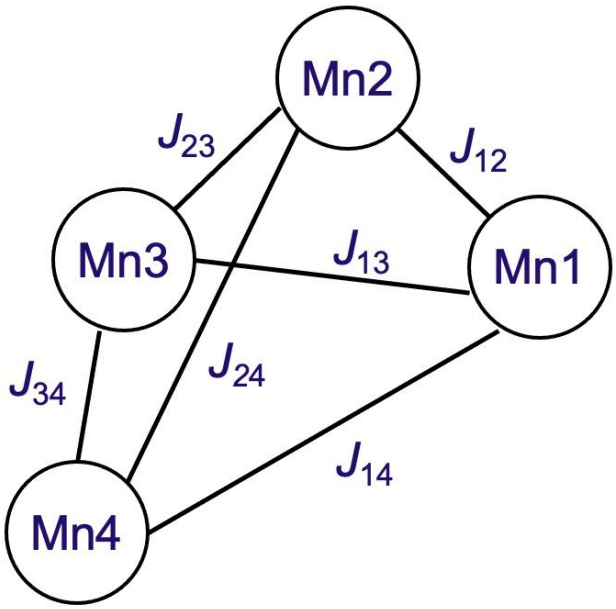

Figure S9. Exchange coupling scheme of the four Mn centers in the OEC.

Table S2. Exchange coupling constants (in cm^{-1}) between Mn centers of the S_2 state in the different protonation-state models.

Exchange Coupling constants	**Model A: W_1OH W_2OH_2 D61COOH**	**Model B: W_1OH_2 W_2OH_2 D61COO**	**Model C: W_1OH_2 W_2OH D61COOH**
J12	-17.4	-16.8	-18.7
J13	6.2	3.3	2.4
J14	2.2	2.4	2.9
J23	20.2	18.3	14.3
J24	1.8	2.3	2.3
J34	-22.6	-23.5	-22.7

Table S3. Spin projection factors of model **A**.

	$\langle S_{Z,A}\rangle_{GS}$	S_A	$\langle S_Z\rangle_{BS}$	S_{tot}	c_A	$k=\left(\frac{\langle S_Z\rangle_{BS}}{S_A}\right)$	k(dimer)
1	0.978	2.0	0.5	0.5	1.956	0.489	0.500
2	-0.497	1.5	0.5	0.5	-0.994	0.331	0.333
3	-0.364	1.5	0.5	0.5	-0.728	0.243	0.333
4	0.383	1.5	0.5	0.5	0.766	0.255	0.333

Table S4. Spin projection factors of model **B**.

	$\langle S_{Z,A}\rangle_{GS}$	S_A	$\langle S_Z\rangle_{BS}$	S_{tot}	c_A	$k=\left(\frac{\langle S_Z\rangle_{BS}}{S_A}\right)$	k(dimer)
1	0.800	2.0	0.5	0.5	1.600	0.400	0.500
2	-0.482	1.5	0.5	0.5	-0.963	0.321	0.333
3	-0.499	1.5	0.5	0.5	-0.999	0.333	0.333
4	0.681	1.5	0.5	0.5	1.362	0.454	0.333

Table S5. Spin projection factors of model **C**.

	$\langle S_{Z,A}\rangle_{GS}$	S_A	$\langle S_Z\rangle_{BS}$	S_{tot}	c_A	$k=\left(\frac{\langle S_Z\rangle_{BS}}{S_A}\right)$	k(dimer)
1	0.883	2	0.5	0.5	1.767	0.442	0.500
2	-0.490	1.5	0.5	0.5	-0.980	0.327	0.333
3	-0.461	1.5	0.5	0.5	-0.922	0.307	0.333
4	0.567	1.5	0.5	0.5	1.135	0.378	0.333

Table S6. Calculated hyperfine coupling constants (MHz) of different protonation state models.

Hydrogen Atoms	**A_{iso}**	**Assignment**
A) OH^-, OH_2, COOH		
H(W2)	1.3	H^{I}
H_{E1}(His332)	-0.7	H^{II}
H(W1)	4.2	H^{III}
H_{E2}(His337)	0.1	H^{IV}
H(Wx)	-0.3	H^{V}
B) OH_2, OH_2, COO^-		
H(W2)	1.8	H^{I}
H_{E1}(His332)	-0.6	H^{II}
H(W1)	1.7	H^{III}
H_{E2}(His337)	0.1	H^{IV}
H(Wx)	-0.1	H^{V}
C) OH_2, OH^-, COOH		
H(W2)	7.7	H^{III}
H_{E1}(His332)	-0.7	H^{II}
H(W1)	1.1	H^{I}
H_{E2}(His337)	0.1	H^{IV}
H(Wx)	0.0	H^{V}
Experimental		
H^{I}	±1.8 (± 0.4)	
H^{II}	±0.1 (± 0.4)	
H^{III}	±2.6 (± 0.2)	
H^{IV}	±0.2 (± 0.2)	
H^{V}	±0.4 (± 0.6)	

Table S7. Calculated isotropic proton hyperfine coupling constants (HFCs) of the S_2 state by straight and Boltzmann averaging over protonation-state structures **A** and **B**. Also shown are the experimental hyperfine coupling constants that were previously measured by 2D HYSCORE spectroscopy and their tentative assignments.

Atoms	Aiso (MHz)	Aiso (MHz)	Aiso (MHz)	Assignment
	A + B	Boltzmann Average[a]	Expt.[b]	
H(W2)	1.5	1.5	±1.8 (± 0.4)	H^{I}
H_{E1}(His332)	-0.7	-0.7	±0.1 (± 0.4)	H^{II}
H(W1)	3.0	3.3	±2.6 (± 0.2)	H^{III}
H_{E2}(His337)	0.1	0.1	±0.2 (± 0.2)	H^{IV}
H(Wx)	-0.2	-0.2	±0.4 (± 0.6)	H^{V}

[a] Boltzmann average is taken at T = 200 K when the S_1-to-S_2 transition was advanced under illumination in experimental measurements..
[b] Experimental isotropic proton HPCs from *Energy & Environ. Sci.* **2012,** *5*, 7747-7756.

Table S8. Calculated isotropic proton hyperfine coupling constants (HFCs, in MHz) of the S_2 state of model **C'**, experimental HFCs (in MHz) and their tentative assignments.

Atoms	C'[a]	Expt.[b]	Assignment
H(W1)	-1.3	±1.8 (± 0.4)	H^{I}
H_{E1}(His332)	-0.6	±0.1 (± 0.4)	H^{II}
H(W2)	-5.9	±2.6 (± 0.2)	H^{III}
H_{E2}(His337)	-0.1	±0.2 (± 0.2)	H^{IV}
H(Wx)	0.1	±0.4 (± 0.6)	H^{V}

[a] Deprotonated model of the S_2 state with W1 = H_2O, W2 = OH^-, and D61 = COO^- (model C')
[b] Experimental isotropic proton HPCs from *Energy & Environ. Sci.* **2012,** *5*, 7747-7756.

4. References in SI:

1. Askerka, M.; Wang, J.; Brudvig, G. W.; Batista, V. S., Structural Changes in the Oxygen-Evolving Complex of Photosystem II Induced by the S1 to S2 Transition: A Combined XRD and QM/MM Study. *Biochemistry* **2014,** *53*, 6860-6862.
2. Umena, Y.; Kawakami, K.; Shen, J.-R.; Kamiya, N., Crystal structure of oxygen-evolving photosystem II at a resolution of 1.9 Å. *Nature* **2011,** *473*, 55-60.
3. Dapprich, S.; Komáromi, I.; Byun, K. S.; Morokuma, K.; Frisch, M. J., A new ONIOM implementation in Gaussian98. Part I. The calculation of energies, gradients, vibrational frequencies and electric field derivatives1Dedicated to Professor Keiji Morokuma in celebration of his 65th birthday.1. *Journal of Molecular Structure: THEOCHEM* **1999,** *461-462*, 1-21.

4. Chung, L. W.; Sameera, W. M. C.; Ramozzi, R.; Page, A. J.; Hatanaka, M.; Petrova, G. P.; Harris, T. V.; Li, X.; Ke, Z.; Liu, F.; Li, H.-B.; Ding, L.; Morokuma, K., The ONIOM method and Its applications. *Chem. Rev.* **2015,** *115*, 5678-5796.
5. M. J. Frisch; G. W. Trucks; H. B. Schlegel; G. E. Scuseria; M. A. Robb; J. R. Cheeseman; G. Scalmani; V. Barone; G. A. Petersson; H. Nakatsuji; X. Li; M. Caricato; A. V. Marenich; J. Bloino; B. G. Janesko; R. Gomperts; B. Mennucci; H. P. Hratchian; J. V. Ortiz; A. F. Izmaylov; J. L. Sonnenberg; D. Williams-Young; F. Ding; F. Lipparini; F. Egidi; J. Goings; B. Peng; A. Petrone; T. Henderson; D. Ranasinghe; V. G. Zakrzewski; J. Gao; N. Rega; G. Zheng; W. Liang, M. H., M. Ehara, K. Toyota, R. Fukuda,; J. Hasegawa, M. I., T. Nakajima, Y. Honda, O. Kitao, H. Nakai,; T. Vreven, K. T., J. A. Montgomery, Jr., J. E. Peralta,; F. Ogliaro, M. J. B., J. J. Heyd, E. N. Brothers, K. N. Kudin,; V. N. Staroverov, T. A. K., R. Kobayashi, J. Normand,; K. Raghavachari, A. P. R., J. C. Burant, S. S. Iyengar,; J. Tomasi, M. C., J. M. Millam, M. Klene, C. Adamo, R. Cammi,; J. W. Ochterski, R. L. M., K. Morokuma, O. Farkas,; J. B. Foresman, a. D. J. F. *Gaussian 16, Revision B.01*, Gaussian, Inc.: Wallingford CT, 2016.
6. Stephens, P. J.; Devlin, F. J.; Chabalowski, C. F.; Frisch, M. J., Ab Initio Calculation of Vibrational Absorption and Circular Dichroism Spectra Using Density Functional Force Fields. *The Journal of Physical Chemistry* **1994,** *98*, 11623-11627.
7. Hay, P. J.; Wadt, W. R., Ab initio effective core potentials for molecular calculations. Potentials for K to Au including the outermost core orbitals. *The Journal of Chemical Physics* **1985,** *82*, 299-310.
8. Hehre, W. J.; Ditchfield, R.; Pople, J. A., Self—Consistent Molecular Orbital Methods. XII. Further Extensions of Gaussian—Type Basis Sets for Use in Molecular Orbital Studies of Organic Molecules. *The Journal of Chemical Physics* **1972,** *56*, 2257-2261.
9. Francl, M. M.; Pietro, W. J.; Hehre, W. J.; Binkley, J. S.; Gordon, M. S.; DeFrees, D. J.; Pople, J. A., Self-consistent molecular orbital methods. XXIII. A polarization-type basis set for second-row elements. *The Journal of Chemical Physics* **1982,** *77*, 3654-3665.
10. Cornell, W. D.; Cieplak, P.; Bayly, C. I.; Gould, I. R.; Merz, K. M.; Ferguson, D. M.; Spellmeyer, D. C.; Fox, T.; Caldwell, J. W.; Kollman, P. A., A Second Generation Force Field for the Simulation of Proteins, Nucleic Acids, and Organic Molecules. *Journal of the American Chemical Society* **1995,** *117*, 5179-5197.
11. Rehr, J. J.; Albers, R. C., Theoretical approaches to x-ray absorption fine structure. *Reviews of Modern Physics* **2000,** *72*, 621-654.
12. Newville, M., IFEFFIT : interactive XAFS analysis and FEFF fitting. *Journal of Synchrotron Radiation* **2001,** *8*, 322-324.
13. Marston, C. C.; Balint-Kurti, G. G., The Fourier grid Hamiltonian method for bound state eigenvalues and eigenfunctions. *The Journal of Chemical Physics* **1989,** *91*, 3571-3576.
14. Spitznagel, G. W.; Clark, T.; von Ragué Schleyer, P.; Hehre, W. J., An evaluation of the performance of diffuse function-augmented basis sets for second row elements, Na-Cl. *J. Comput. Chem.* **1987,** *8*, 1109-1116.
15. Clark, T.; Chandrasekhar, J.; Spitznagel, G. W.; Schleyer, P. V. R., Efficient diffuse function-augmented basis sets for anion calculations. III. The 3-21+G basis set for first-row elements, Li–F. *J. Comput. Chem.* **1983,** *4*, 294-301.
16. Grimme, S.; Antony, J.; Ehrlich, S.; Krieg, H., A consistent and accurate ab initio parametrization of density functional dispersion correction (DFT-D) for the 94 elements H-Pu. *J. Chem. Phys.* **2010,** *132*, 154104.
17. Neese, F., The ORCA program system. *WIREs Comput. Mol. Sci.* **2012,** *2*, 73-78.

18. van Lenthe, E.; Baerends, E. J.; Snijders, J. G., Relativistic total energy using regular approximations. *J. Chem. Phys.* **1994,** *101*, 9783-9792.
19. van Wüllen, C., Molecular density functional calculations in the regular relativistic approximation: Method, application to coinage metal diatomics, hydrides, fluorides and chlorides, and comparison with first-order relativistic calculations. *J. Chem. Phys.* **1998,** *109*, 392-399.
20. Eichkorn, K.; Treutler, O.; Öhm, H.; Häser, M.; Ahlrichs, R., Auxiliary basis sets to approximate Coulomb potentials. *Chem. Phys. Lett.* **1995,** *240*, 283-290.
21. Eichkorn, K.; Weigend, F.; Treutler, O.; Ahlrichs, R., Auxiliary basis sets for main row atoms and transition metals and their use to approximate Coulomb potentials. *Theor. Chem. Acc.* **1997,** *97*, 119-124.
22. Weigend, F., Accurate Coulomb-fitting basis sets for H to Rn. *Phys. Chem. Chem. Phys.* **2006,** *8*, 1057-1065.
23. Grimme, S.; Ehrlich, S.; Goerigk, L., Effect of the damping function in dispersion corrected density functional theory. *J. Comput. Chem.* **2011,** *32*, 1456-1465.
24. Pantazis, D. A.; Ames, W.; Cox, N.; Lubitz, W.; Neese, F., Two Interconvertible Structures that Explain the Spectroscopic Properties of the Oxygen-Evolving Complex of Photosystem II in the S2 State. *Angew. Chem. Int. Ed.* **2012,** *51*, 9935-9940.
25. Cox, N.; Retegan, M.; Neese, F.; Pantazis, D. A.; Boussac, A.; Lubitz, W., Electronic structure of the oxygen-evolving complex in photosystem II prior to O-O bond formation. *Science* **2014,** *345*, 804-808.
26. Cox, N.; Ames, W.; Epel, B.; Kulik, L. V.; Rapatskiy, L.; Neese, F.; Messinger, J.; Wieghardt, K.; Lubitz, W., Electronic Structure of a Weakly Antiferromagnetically Coupled MnIIMnIII Model Relevant to Manganese Proteins: A Combined EPR, 55Mn-ENDOR, and DFT Study. *Inorg. Chem.* **2011,** *50*, 8238-8251.
27. Pantazis, D. A.; Orio, M.; Petrenko, T.; Zein, S.; Bill, E.; Lubitz, W.; Messinger, J.; Neese, F., A New Quantum Chemical Approach to the Magnetic Properties of Oligonuclear Transition-Metal Complexes: Application to a Model for the Tetranuclear Manganese Cluster of Photosystem II. *Chem. Eur. J.* **2009,** *15*, 5108-5123.